

Impact of Ni/Co in perovskites as catalysts for syngas production via methane reforming with CO₂

Impacto de Ni/Co en perovskitas como catalizadores para producir syngas por reformado de metano con CO₂

Lugo, Claudio^{1*}; Torres, Ruben¹; Guerrero, Maryuri¹; Fereira, Carla¹; Petit, Eliel¹; Pérez, Patricia²; Rondón, Jairo³

¹Laboratorio de Cinética y Catálisis, Departamento de Química, Facultad de Ciencias, Universidad de Los Andes, Mérida, Venezuela.

²Laboratorio de Polímeros, Departamento de Química, Facultad de Ciencias, Universidad de Los Andes, Mérida, Venezuela.

³Biomedical & Chemical Engineering Departments, Polytechnic University of Puerto Rico, San Juan, Puerto Rico, USA.

[*claudiolugo@ula.ve](mailto:claudiolugo@ula.ve)

Abstract

Layered perovskite-type mixed oxides $A_{n+1}B_nX_{3n+1}$ ($A = Sr/Ba$; $B = Co/Ni$; $X = O$) were synthesized via solution combustion synthesis (SCS) assisted by microwave radiation. These materials were characterized using advanced techniques such as Fourier-transform infrared spectroscopy (FTIR) and X-ray diffraction (XRD). FTIR analysis revealed distinctive signals corresponding to metal-oxygen (M-O) interactions at low wavelengths. XRD identified the primary phase as a layered La_2NiO_4 perovskite with a tetragonal structure ($n=1$) formed during the glycine combustion. This technique also allowed the calculation of crystallite sizes, with values below 100 nm for all samples. Regarding their catalytic performance, the mixed oxides exhibited remarkable thermal stability and resistance to sintering and deactivation by carbon deposition during the dry reforming of methane. The P-NiCo-R4 perovskite stood out among the samples studied, achieving the highest methane conversion at 78.68%.

Keywords: Mixed oxides, perovskites, methane reforming, environmental pollution.

Resumen

Se sintetizaron óxidos mixtos tipo perovskitas en capas $A_{n+1}B_nX_{3n+1}$ ($A = Sr/Ba$; $B = Co/Ni$; $X = O$) mediante combustión en solución (SCS) asistida por radiación de microondas. Estos materiales fueron caracterizados utilizando técnicas avanzadas como la espectroscopía infrarroja por transformada de Fourier (FTIR) y la difracción de rayos X (DRX). El análisis por FTIR reveló señales distintivas de las interacciones metal-oxígeno (M-O) a bajas longitudes de onda. Por su parte, la DRX permitió identificar la fase principal como una perovskita en capas tipo La_2NiO_4 con estructura tetragonal ($n=1$), formada durante el proceso de combustión de la glicina. Además, esta técnica permitió calcular el tamaño de los dominios cristalinos, obteniéndose valores inferiores a 100 nm para todas las muestras. En cuanto a su desempeño catalítico, los óxidos mixtos demostraron una notable estabilidad térmica y resistencia frente a la sinterización y la desactivación por deposición de carbono durante el reformado seco de metano. Entre las muestras estudiadas, la perovskita P-NiCo-R4 destacó por alcanzar la mayor conversión de metano, con un 78,68 %.

Palabras clave: Óxidos mixtos, perovskitas, reformado de metano, contaminación ambiental.

1 Introduction

Currently, various proposals exist to control the emission of environmental pollutants, particularly greenhouse gases like carbon dioxide and methane.

However, these measures do not entirely solve the problem, making it essential to continue developing technologies contributing to environmental regulations.

Natural gas (whose main component is methane) is a strategic resource for global energy supply, accounting for

approximately 23% of total energy demand (IEA 2011; Bonadonna 2020; OPEC 2020). Venezuela, for instance, holds the world's tenth-largest proven natural gas reserve (~5.67 trillion cubic meters), with much of it present as associated natural gas (C.I.A. 2021). Methane extracted in Venezuela contains 80% methane, ethane, propane, and carbon dioxide traces.

Natural gas is significant because it can be converted through secondary processes into synthesis gas or syngas—a mixture of hydrogen and carbon monoxide—used in numerous processes in the petrochemical sector. It is considered one of the cleanest fuels due to its lower production of pollutant gases (CO_2 , NO_x , SO_2) compared to other fossil sources (Edwards *et al.*, 1995).

A secondary route that could play a prominent role in the future of environmental chemistry is the dry reforming of methane (DRM) reaction, where reacting species such as CO_2 and CH_4 are converted into synthesis gas. This process transforms greenhouse gases (negative environmental impact) into a mixture of H_2 and CO with numerous industrial applications (positive impact for humanity) (Haghghi *et al.*, 2007). DRM employs solid heterogeneous catalysts resistant to thermal decomposition.

A practical methodology for obtaining nanostructured materials is solution combustion synthesis (SCS). In this method, a metal precursor in an aqueous solution (nitrate and/or acetate salts) is dissolved in deionized water in a fuel with high metal affinity. SCS offers advantages such as the speed of the method, its simplicity, and its cost-effectiveness, making it suitable for potential industrial applications (Civera *et al.*, 2003; Specchia *et al.*, 2004; Wang *et al.*, 2009; García *et al.*, 2010; Pérez *et al.*, 2015; Lugo *et al.*, 2010-2022-2024.a).

Some advantages of solution combustion synthesis compared to other chemical techniques include:

Utilization of internal chemical energy: SCS relies on the heat generated by exothermic reactions between the fuel and the oxidizer, eliminating the need for external energy sources. This reduces operational costs and enhances the economic efficiency of the process.

Rapid synthesis speed: The process can be completed within minutes due to the high reaction rates, making it ideal for the efficient, large-scale production of advanced materials.

Controlled heat release: Heat generated during combustion is released gradually and uniformly, layer by layer. This prevents thermal damage or deformation of the materials and ensures products with homogeneous properties.

Ease of industrial integration: The simplicity, scalability, and cost-effectiveness of the process make it highly compatible with industrial production lines, enabling the large-scale fabrication of nanomaterials, catalysts, and

other advanced compounds (Siddique *et al.*, 2022; Rodríguez-Sulbarán *et al.*, 2018).

This research project aimed to prepare mixed oxide perovskites with specific metals such as Ni and Co using solution combustion synthesis (SCS). The physicochemical properties of the different solids were studied using characterization techniques such as FTIR and XRD. These solids were employed as heterogeneous catalysts to study the kinetics of the dry reforming of methane with CO_2 . The reaction was monitored using a gas chromatograph coupled to the main system.

2 Experimental Procedure

2.1 Perovskite Synthesis

The materials (mixed oxides) were prepared using solution combustion synthesis (SCS), as described by Patil (Patil *et al.*, 1997-2002), Mukasyan (Mukasyan *et al.*, 2001-2007), and Varma (Varma *et al.*, 2003). This methodology was revised and validated in the Kinetics and Catalysis Laboratory at the University of Los Andes by Pérez (Pérez *et al.*, 2015), Briceño (Briceño *et al.*, 2018), and Lugo (Lugo *et al.*, 2022-2024.b).

2.1.1 Synthesis Methodology

The precursor mixture was placed in a modified porcelain crucible with a lid, allowing the gases generated during fuel combustion to escape. The crucible was then transferred to a household microwave oven (Premium brand, model PM7078, 700W power), where radiation was applied at 80% power (Zhao *et al.*, 2004).

Combustion of the precursor mixture began approximately 35 seconds after the start of radiation and lasted an additional 15 seconds. During this time, intense flames and a large volume of gases were generated due to the ionization of the accumulated gases inside the crucible, significantly increasing the system's temperature. The total radiation time for the precursor mixture was approximately 95 seconds. The final product was a fine, grayish powder identified as the mixed oxide perovskite.

2.1.2 Stoichiometry

Table 1 presents the different perovskites prepared via SCS.

Figure 1 shows the combustion process of the precursor mixture and the unground material obtained after combustion. 5

Table 1. Layered perovskite-type oxides $A_{n+1}B_nO_{3n+1}$ ($A = Sr/Ba$; $B = Ni/Co$) synthesized via SCS.

Formula ($A_{n+1}B_nO_{3n+1}$)	Ignition	Code
$Sr_{1.5}Ba_{0.5}CoO_4$	Microwave	P-Co-R1
$Sr_{1.5}Ba_{0.5}Ni_{0.5}Co_{0.7}O_4$		P-NiCo-R2
$Sr_{1.5}Ba_{0.5}Ni_{0.5}Co_{0.5}O_4$		P-NiCo-R3
$Sr_{1.5}Ba_{0.5}Ni_{0.7}Co_{0.3}O_4$		P-NiCo-R4
$Sr_{1.5}Ba_{0.5}NiO_4$		P-Ni-R5



Fig. 1. Step-by-step SCS synthesis of perovskites: 1.- Gel formation, 2.- Gel/crucible (before radiation) and final product, 3.- Before microwave, and 4.- After grinding.

2.2 Characterization

The synthesized materials were characterized using two quantitative techniques:

- I. Fourier Transform Infrared Spectroscopy (FTIR): Analysis was performed using a Perkin Elmer Frontier FTIR spectrophotometer.
- II. X-ray Diffraction (XRD): Powder diffraction measurements were conducted using a Bruker D8 Advance diffractometer with Cu K α radiation (wavelength 1.5406 Å). The instrument operated at 40 kV and 40 mA. Data were collected over a 2 θ range of 2°–70°, with a step time of 0.6 seconds and a step size of 0.02035°.

3 Discussion and Results

3.1 Infrared Spectroscopy, FTIR

The infrared spectra of $A_{n+1}B_nO_{3n+1}$ perovskites ($n = 0.0$ – 0.3 – 0.5 – 0.7 – 1.0) with $A = Sr/Ba$ and $B = Ni/Co$, prepared via SCS, are shown in Figure 2. In the NiCo-R series, a broad

band near 3440.7 cm $^{-1}$ is observed, attributed to the symmetric and asymmetric stretching of the O-H bond, corresponding to coordinated water molecules in the mixed oxides (Ramos *et al.*, 2015; Neira *et al.*, 2016). Two small signals between 2925 and 2855 cm $^{-1}$ are the result of –CH $_2$ –C=O stretching vibrations with sp 3 hybridization; these groups originate from an excess of fuel during material synthesis (Wade 2004).

The moderately broad band at 1631.9 cm $^{-1}$ corresponds to the asymmetric deformation of the carboxylate ion COO-M, a species involved in the material synthesis (Hernández *et al.*, 2006). The peak around ~1461 cm $^{-1}$ is due to the asymmetric stretching vibrations of nitrates (NO $_3$ $^-$) from the synthesis process or carbonates (CO $_{3}^{2-}$) absorbed from the atmosphere (Gao *et al.*, 2012; Silva *et al.*, 2015; Darroudia *et al.*, 2016; Song *et al.*, 2016).

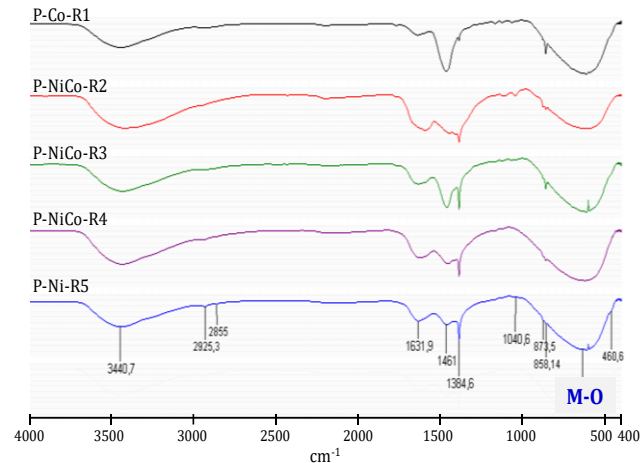


Fig. 2. FTIR Infrared Spectra of Layered Perovskite-Type Oxides $A_{n+1}B_nO_{3n+1}$ with $A = Sr/Ba$ and $B = Ni/Co$.

The signal at 1384.6 cm $^{-1}$ may correspond to the symmetric stretching mode of the N-O bond (NO $_2$), associated with bidentate coordination compounds (Rendón *et al.*, 2006). The small signal observed at 1040.6 cm $^{-1}$ is attributed to the in-plane bending vibration of the C-O bond, associated with acetals and saturated aliphatic primary alcohols (Gómez 2010).

In the fingerprint region of M-O interactions (at lower wavelengths), characteristic signals of the allowed vibrational modes associated with the metals and non-metals used are observed: Co $^{+2}$, Ni $^{+2}$, Sr $^{+2}$, and Ba $^{+2}$, with OH groups and oxygen atoms bonded to these metals (O-M-O) (Anacona *et al.*, 2013). The low-intensity peak near 873.5 cm $^{-1}$ corresponds to vibrations of the Sr-O bond in an octahedral site (Sithole *et al.*, 2017; Briceño *et al.*, 2020). The band at 858.14 cm $^{-1}$ is attributed to the vibrational formation of the cubic Ba-O bond (Villaquirán *et al.*, 2015).

At 660 cm $^{-1}$, several signals may be present, corresponding to Sr $^{+2}$ -O bond vibrations (Neira *et al.*, 2016) or to vibrations of the face-centered cubic phase of the Ni-O

bond (Liu *et al.*, 2013). The Co-O bond's stretching vibrations are also located near 660 cm^{-1} (Radev *et al.*, 2008). In the far-infrared region, between $460\text{--}450\text{ cm}^{-1}$, a small peak is observed, which may correspond to vibrations of the

Ni-O bond (Rahdar *et al.*, 2015; Gao *et al.*, 2012) and/or asymmetric vibrations of the Sr-O bond (Sultana *et al.*, 2015).

Table 2. Band Assignment of FTIR Spectra for Layered Perovskites $A_{n+1}B_nO_{3n+1}$

v (Ref.)	v (cm^{-1})	Bond	Assignment
3440	3440.7	O-H	Symmetric and asymmetric stretching of the O-H group
3050-2870	2925-2855	$\text{CH}_2\text{-C=O}$	Stretching vibrations of $-\text{CH}_2\text{-C=O}$ with sp^3 hybridization
1650-30	1631.9	COO^-M	Asymmetric deformation of the carboxylate ion (COO^-M)
1470-40	1461	N-O/C-O	Asymmetric stretching vibrations of nitrates (NO_3^-) and/or carbonates (CO_3^{2-})
1384	1384.6	N-O	Symmetric tension of NO_2 (N-O bond) associated with bidentate coordination compounds
1040	1040.6	C-O	In-plane bending vibration of the C-O bond, associated with acetals and saturated aliphatic primary alcohols
Fingerprint region of M-O interactions (low wavelength)			
862	873.5	Sr-O	Bending vibrations of the Sr-O bond
860	858.14	Ba-O	Formation vibrations of the Ba-O bond
660	~660	Ni-O	Vibrations of the face-centered cubic phase of the Ni-O bond
	~660	Sr-O	Vibrations of the $\text{Sr}^{+2}\text{-O}$ bond
678	~660	Co-O	Stretching vibration of the Co-O bond
470	~460	Ni-O	Vibration of the Ni-O bond
450	~450	Sr-O	Asymmetric vibration of the Sr-O bond

3.2 X-Ray Diffraction (XRD)

Figure 3 displays the diffraction patterns of the layered perovskites $A_{n+1}B_nO_{3n+1}$ ($n = 0.0, 0.3, 0.5, 0.7, 1.0$) with $A = \text{Sr/Ba}$ and $B = \text{Ni/Co}$. Identifying the phase(s) present in the synthesized materials required using the XPert HighScore Plus 2.1 software and the PDF2-2004 database from the ICDD (Takeda *et al.*, 1990).

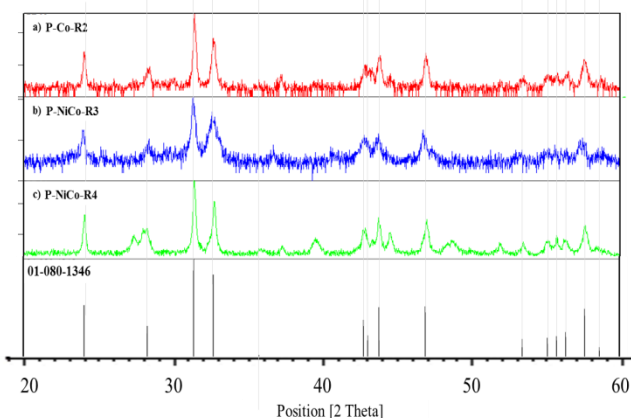


Fig. 3. Diffraction patterns of the layered perovskites of the type $A_{n+1}B_nO_{3n+1}$. Card: 01-070-1333 (La_2NiO_4 Perovskite).

The formation of the perovskite phase is favored when glycine is used as a fuel, as it promotes higher temperatures during the combustion process, inducing the formation of the perovskite phase (Pérez M. *et al.*, 2015). It is important to note that heating to very high temperatures can break the perovskite structure, forming metallic phases known as

Ruddlesden-Popper phases. These phases tend to form layered perovskites of the type $A_{n+1}B_nO_{3n+1}$ (Savinskaya *et al.*, 2007).

The perovskite phase identified using the PDF2-2004 database from the ICDD (technical card: 01-070-1333) suggests a layered perovskite structure, $A_{n+1}B_nO_{3n+1}$ ($n = 1$), specifically La_2NiO_4 . This ceramic material forms due to vacancy defect formation during its synthesis at high temperatures (Askeland & Phulé, 2004).

3.2.1 Calculation of Crystalline Domain

The crystalline domain size in the synthesized oxides was determined using the Scherrer equation (Eq. 01) (Langford *et al.*, 1978).

$$\beta = \frac{(0.89) \cdot \lambda}{FWHM(S) \cdot (\cos 2\theta)} \quad (\text{Eq. 01})$$

β = Crystalline domain size.

λ = Wavelength of the radiation used (λCu) in nm.

$FWHM(S)$ = Full width at half maximum of the diffraction peak at angle θ .

$$FWHM(S) = \frac{SF \times A}{l} \quad (\text{Eq. 02})$$

SF = Constant related to the shape of the profile, approximately 0.85.

A = Sum of the net intensity of all points forming the diffraction peak.

l = Height of the diffraction peak at angle θ .

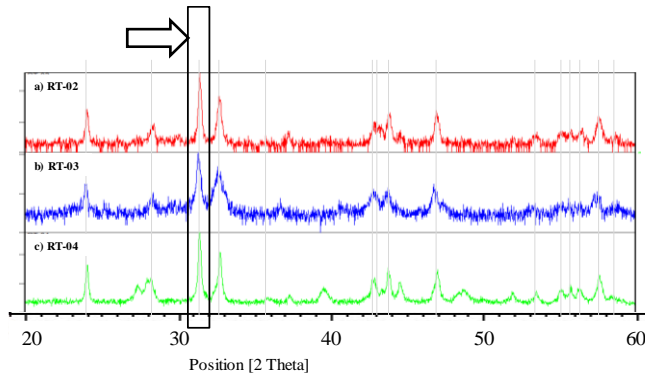


Fig. 4. hkl (103) line peak in XRD used to calculate the crystalline domain size of the material (perovskite).

For all cases, the (103) line of the diffraction pattern was selected. This equation relates the width and intensity of the peaks to the domain size; the integrated peak width (FWHM) of the signal is inversely proportional to the crystalline domain size (β). For this calculation, the peak with the highest intensity of the dominant phase present in the obtained oxides was selected (Fig. 4).

Table 3 presents the crystalline domain size, determined using the Scherrer equation (Eqs. 01–02). It can be observed that the prepared solids have an average crystalline domain size below the range considered as nanoparticles, i.e., diameters smaller than 100 nm.

Table 3. Parameters Used in the Scherrer Equation and Determined Crystalline Domain Diameters.

Code	SF	Area	Height	k	λ (Cu)	2θ	cos2θ	FWHM(S)	d (nm)
P-NiCo-R2	0.85	209.8	956.6	1.00	1.54	31.437	0.9998	0.163600	8.379
				0.89			0.9998	0.092711	16.614
P-NiCo-R3	0.85	256.4	996.7	1.00	1.54	31.430	0.9999	0.159400	8.599
				0.89			0.9999	0.090315	17.053
P-NiCo-R4	0.85	234.1	1034.6	1.00	1.54	31.417	1.0000	0.142300	9.632
				0.89			1.0000	0.080616	19.103

3.3 Catalytic Test: Dry Reforming of Methane

3.3.1 Instrumental Response (Gas Chromatography)

For a Gas Chromatograph (GC), the thermal conductivity detector (TCD) response factor was determined using Argon as the carrier gas at a 30 mL/min flow rate through the system's internal column setup.

Table 4. TCD Response Coefficients for Each Gas.

Gas Substance	TCD Response Factor (relative to CO)
Hydrogen, H ₂	8.29
Methane, CH ₄	3.76
Carbon Dioxide, CO ₂	1.26
Carbon Monoxide, CO	1.00

The GC oven operated under isothermal conditions at approximately 150 °C. A different response factor was verified for each compound (Table 4).

3.3.2 Pretreatment

The synthesized layered perovskites were pretreated with a hydrogen flow at a rate of 30 mL/min, using a heating ramp of 10°C/min, from room temperature to 700°C. The temperature was maintained at 700°C for approximately 15 minutes (Fig. 5).

3.3.3 Calibration (Gas Chromatography)

The most significant parameters of the dry reforming of methane (DRM) reaction and gas chromatography (GC) were calibrated, including mass, reactant flow, temperature range, and space velocity, for the kinetic regime of the reaction. The ideal conditions to study the kinetics of the proposed catalysts for the reaction system are shown in Table 5.

Table 5. Actual Conditions for Gas Chromatography Analysis

Parameter	Value
Catalyst Mass (mg)	≥ 0.030
Total Flow (mL/min)	≥ 50
Temperature Range (°C)	700
Space Velocity Range x10 ⁻³ (mL/g.h)	120–240

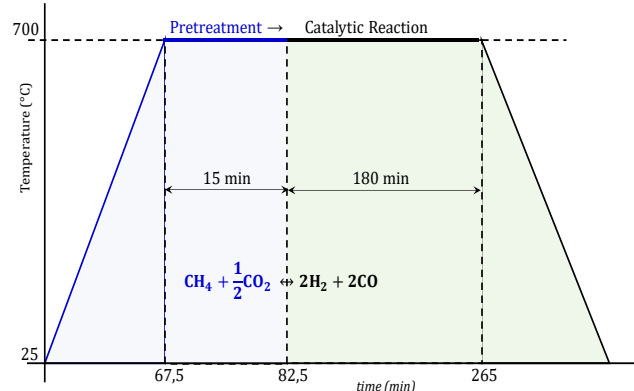


Fig. 5. Thermal cycle for pretreatment/analysis in DRM using layered perovskites as catalysts.

3.3.4 Reaction Conditions

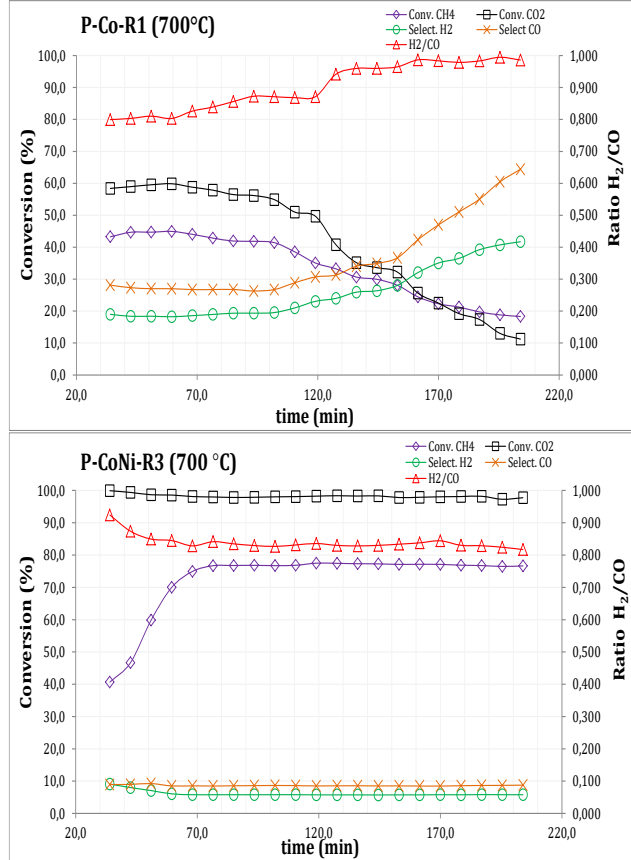
Approximately 30 mg of perovskite (heterogeneous catalyst for the DRM reaction) are initially weighed and placed in a U-shaped quartz reactor. The reaction is conducted at a fixed temperature of 700°C. The molar ratio of the reactant species CH₄/CO₂ in the feed is 1:1, with a total volumetric flow of 40 mL/min and a space velocity of 120,000 mL/g·h.

3.3.5 Catalytic Results for DRM

The methane and carbon dioxide conversions, selectivity's toward syngas, and the H₂/CO molar ratio for the P-NiCo-R perovskites at 700°C are shown in Figure 6.

It was observed that the partial substitution and combination of cobalt with nickel tend to enhance the catalytic activity in the DRM reaction and the selectivity toward syngas formation (Fig. 6). Almost all the perovskites used as heterogeneous catalysts in DRM exhibited good thermal stability over a reaction period of ~200 minutes, indicating resistance to sintering and minimal deactivation due to carbon deposition. This stability is attributed to:

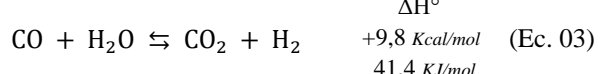
I. The small particle size, particularly the average size



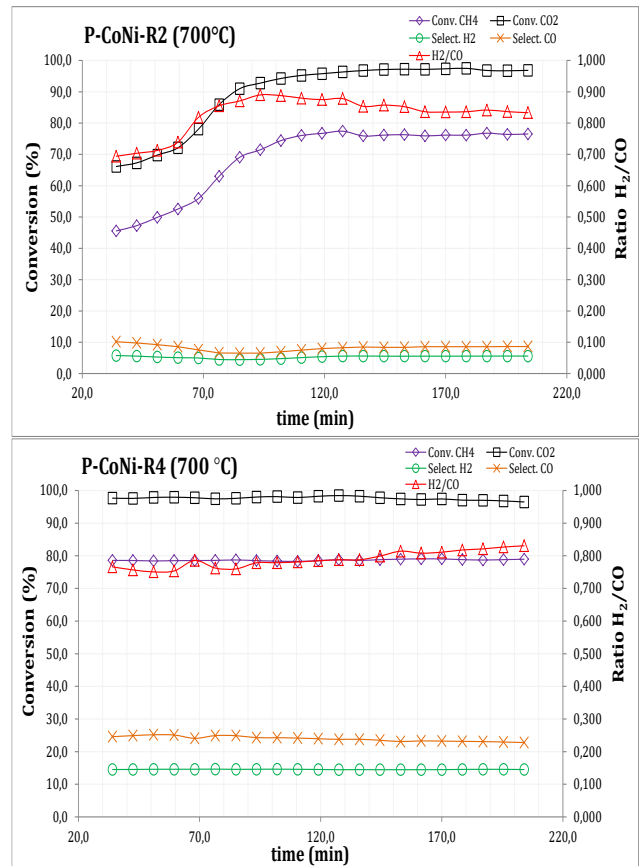
of nickel, and

II. The strong interactions of metallic sites with the structure at high temperatures (Sierra *et al.*, 2009; García *et al.*, 2010).

The conversion of carbon dioxide is favored over methane in all P-NiCo-RT series solids due to simultaneous competitive reactions, such as the reverse water-gas shift reaction. In this reaction, CO₂ reacts with the H₂ formed to produce CO and water vapor (Haghghi *et al.*, 2007) (Eq. 03).



The molar ratio of the products obtained during DRM (H₂/CO) shows values below unity. The reverse water-gas shift reaction (Eq. 03) is likely causing an increase in the amount of CO and, consequently, a decrease in the final product ratio (Lugo *et al.*, 2010).



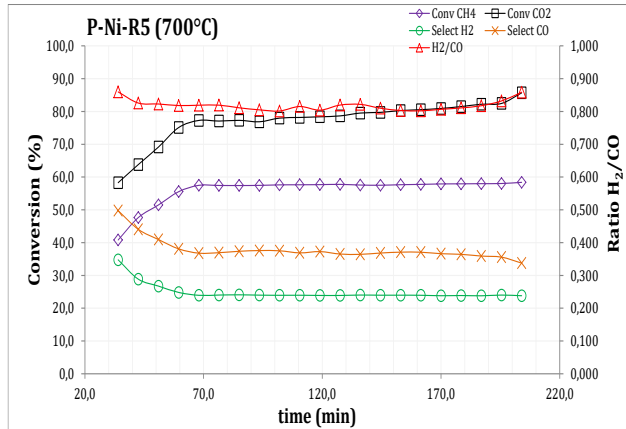


Fig. 6. Methane and CO₂ conversion, syngas selectivity, and H₂/CO ratio for perovskites at 700°C.

Table 6. Average CH₄/CO₂ Conversion (%), H₂/CO Ratio, and Syngas Selectivity for Perovskites at 700°C

Measured Parameter	P/Fe-1	P/NiFe-2	P/NiFe-3	P/NiFe-4	P/Ni-5
CH ₄ Conversion (%)	33.81	68.84	72.55	78.68	56.03
CO ₂ Conversion (%)	41.54	89.43	98.24	97.63	77.18
H ₂ /CO Ratio	0.90	0.83	0.84	0.79	0.82
H ₂ Selectivity (%)	25.88	5.30	6.12	14.55	24.86
CO Selectivity (%)	36.17	8.22	8.64	23.95	37.87
Σ (H ₂ +CO Selectivity %)	62.05	13.52	14.76	38.50	62.73

The selectivity toward the synthesized perovskites' reaction products (H₂ and CO) is moderate to low due to the extreme analysis conditions and competing side reactions for the catalytic metallic sites.

The perovskites with the highest average methane conversion during DRM at 700°C over the entire reaction time (~200 minutes) were:



This observed catalytic behavior is likely due to a synergistic effect between the metals (cobalt and nickel), which significantly enhances the properties of the metallic active sites.

Acknowledgments

Special thanks to the X-Ray Laboratory at the Industrial University of Santander and its director, Professor José Antonio Henao Martínez, for their valuable collaboration in performing the synthesized samples' X-ray Diffraction (XRD) analyses.

4 Conclusion

Mixed oxide perovskites were synthesized via the solution combustion synthesis (SCS) method, using glycine as a fuel and microwave radiation. This method allowed for

the rapid, efficient, and cost-effective production of nanomaterials.

Infrared spectroscopy (FTIR) identified the characteristic bands of M–O bonds, all below 1000 cm⁻¹, some of which were overlapped. When compared with reported values, these results confirmed the effectiveness of the synthesis method.

The diffraction patterns of the bimetallic solids (P-NiCo-R2, P-NiCo-R3, P-NiCo-R4) revealed the presence of a predominant phase corresponding to a tetragonal perovskite-type mixed oxide (space group: I4/mmm), specifically lanthanum nickel oxide (La₂NiO₄), identified using card 01-080-1346 from the PDF2-2004 database of the ICDD. Furthermore, the crystalline domain size (hkl line 103) was determined from XRD using the Scherrer equation, showing that the diameter was below 100 nm in all cases.

The catalytic study of the dry reforming of methane (DRM) demonstrated that the partial substitution of cobalt (Co) with nickel (Ni) enhances the catalytic activity of the reaction, highlighting a synergistic effect between the metals in the B position. Most perovskites exhibited good thermal stability over the reaction period, indicating resistance to sintering and minimal deactivation due to carbon deposition.

Perovskite 1 (P-Co-R1) deactivated during the catalytic test due to poisoning of the active site caused by carbon deposition, showing the precursor influence of Co on hydrocarbons. Perovskite 5 (P-Ni-R5) achieved the highest

selectivity despite moderate conversions of CH₄ and CO₂.

The average methane conversion order for the synthesized perovskites in the DRM reaction was:

P-CoNi-R4	P-CoNi-R3	P-CoNi-R2
78,68 %	> 72,55 %	> 68,84 %

All bimetallic perovskites showed higher methane conversions at 700°C compared to monometallic ones. This suggests the existence of a synergistic effect between Co and Ni, which enhances the conversion.

The conversion of CO₂ was favored over CH₄ in all the prepared catalysts due to the presence of competitive reactions, such as the reverse water-gas shift reaction, which consumes part of the formed products.

The molar ratio of the products (H₂/CO) was less than one in all cases, likely due to secondary reactions occurring during DRM, contributing to an increased CO quantity.

The selectivity toward syngas showed varied percentage values due to the extreme conditions of the analysis and side reactions competing for the metallic sites on the perovskite surface.

5 References

- Anacona, O., García, D., Kiminami, R. y Raigoza, C., (2013). Efecto de la temperatura en la estructura cristalina de polvos cerámicos de K_{0,5}Na_{0,5}NbO₃ obtenidos por el método de reacción por combustión, Revista latinoamericana de Metalurgia y Materiales, Vol. 33 (1), pp. 108-115.
- Askeland, D. y Phulé P., (2004). Ciencia e ingeniería de los materiales. D.F. México: Thomson.
- Briceño, J., Lugo, C., García, E., Rondón, J., Pérez, P., Rodríguez, P., Del Castillo, H. y Imbert, F., (2020). Síntesis de perovskitas basadas en Ni y Fe vía SCS con radiación microondas y su empleo en el reformado seco de metano. Revista Ciencia e Ingeniería, Vol. 41 (2), pp. 205-216.
- Bonadonna, T., (2020). Perspectivas Energéticas 2021-2040. Petróleo y Gas Natural. https://cavecon.org.ve/wp-content/uploads/2020/11/Perspectivas_Energeticas_2021_Petroleo_y_Gas_Natural.pdf
- C.I.A., (2021). Natural gas - proved reserves. The World Factbook. https://www.cia.gov/the-world-factbook/static/3a6e5fc200e47bc5cf68bd3a5d57481b/Energy_World.pdf
- Civera, A., Pavese, M., Saracco, G. y Specchia, V., (2003). Combustion synthesis of perovskite-type catalysts for natural gas combustion. Catalysis Today, Vol. 83, pp. 199-211.
- Darroudia, M., Bagherpour, M., Hosseini, H. y Ebrahimi, M., (2016). Biopolymer-assisted green synthesis and characterization of calcium hydroxide nanoparticles. Ceramics International, Vol. 42 (3), pp. 3816-3819.
- Edwards, J. y Maitra, A., (1995). The chemistry of methane reforming with carbon dioxide and its current and potential applications. *Fuel Processing Technology*, Vol. 42 (2-3), pp. 269-289.
- Gao, H., Wang, G., Yang, M., Tan, L. y Yu, J., (2012). Novel tunable hierarchical Ni-Co hydroxide and oxide assembled from two-wheeled units. *Nanotechnology*, Vol. 23 (1), pp. 1-9.
- García, E., Rondón, J., Belandria, L., Meléndez, H., Lugo, C. y Imbert F., (2010). Dry methane reforming over Ni-Co supported by impregnation on MgO nanoparticles, *Revista Ciencia e Ingeniería*, Vol. 31 (2), pp. 77-82.
- Gómez, J., (2010). Síntesis y caracterización del sistema LaSrCrFeO₃ soportado sobre óxidos de cerio dopados con elementos de transición interna. Tesis Doctoral en Ciencias Química, Departamento de Química, Facultad de Ciencias, Universidad Nacional de Colombia, Bogotá, Colombia, pp. 156-158.
- Haghghi M., Sun Z., Wu J., Bromly J., Wee H.L., Ng E., Wang Y., Zhang D., (2007). On the reaction mechanism of CO₂ reforming of methane over a bed of coal char, *Proceedings of the Combustion Institute*, Vol. 31 (2), pp. 1983-1990.
- Hernández, J., Castillo, S., Esparza, H., Téllez, E. y Duarte, J., (2006). Síntesis y caracterización de nano-mono cristales de Glicina-Nitrato de Sodio, GSN, con propiedades ópticas no-lineales. *Tecnura*, Vol. 9 (18), pp. 4-9.
- International Energy Agency, IEA, World Energy Outlook 2011, Paris, (2011), OECD/IEA.
- Langford, J. y Wilson, A., (1978). Scherrer after sixty years: A survey and some new results in the determination of crystallite size. *Journal of Applied Crystallography*, Vol. 11, pp. 102-113.
- Liu, L., Guo, Y., Wang, Y., Guo, H., (2013). Hollow NiO nanotubes synthesized by bio-templates as the high-performance anode materials of lithium-ion batteries. *Electrochimica Acta*, Vol. 114, 42-47
- Lugo, C., García, E., Rondón, J., Meléndez, H., Pérez, P. y Del Castillo, H., (2010). Síntesis de óxidos mixtos de Co, Ni y Cu sobre MgO por el método de combustión con urea y estudio en la reacción de reformado seco de metano con CO₂. *Revista Ciencia e Ingeniería*, Vol. 31 (1), pp. 53-59.
- Lugo, C., Rosal, H., Hidalgo, J., Rondón, J., Pérez, P., Rodríguez, P., Del Castillo, H. y Imbert, F., (2022). Preparation of single and layered Perovskites (A = La and Sr/Ca; B = Ni/Co and Ni/Al) from solution combustion synthesis, SCS, via microwave radiation. *Revista Ciencia e Ingeniería*, Vol. 43 (3), pp. 245-256.
- Lugo C., Fereira C., Petit E., Guerrero M., Torres R., Pérez P., Rodríguez P., Rondón J., (2024.a). Estudio catalítico sobre RSM empleando óxidos mixtos Perovskitas Sr_{0,7}Mg_{0,3}Ni_xCo_{1-x}O₃, obtenidas vía combustión en

- solución, SCS. Revista Ciencia e Ingeniería, Vol. 45 (2), pp. 169-178.
- Lugo C., Petit E., Guerrero M., Torres R., Fereira C., Pérez P., Rondón J., (2024.b). Síntesis de perovskitas en capas tipo $A_{n+1}B_nX_{3n+1}$ ($A=$ Sr/Mg; $B=$ Ni/Fe; $X=$ O) vía SCS con Actividad Catalítica en el Reformado seco de metano. Revista Ciencia e Ingeniería, Vol. 45 (3), pp. 265-274.
- Mukasyan, A., Costello, C., Sherlock, K., Lafarga, D., y Varma, A., (2001). Perovskite Membranes by Aqueous Combustion Synthesis: Synthesis and Properties. Separation and Purification Technology, Vol. 25 (1-3), pp. 117-126.
- Mukasyan, A., Epstein, P. y Dinka, P., (2007). Solution combustion synthesis of nanomaterials. Proceedings of the Combustion Institute, Vol. 31 (2), pp. 1789-1795.
- Neira, A., Gómez, J. y Vera, E., (2016). Synthesis and characterization of a simple $La_{0.8}Sr_{0.2}CrO_3$ perovskite (Universidad del Valle). Revista de Ciencias, Vol. 20 (1), pp. 79-94.
- Patil, K., Aruna, S. y Ekambaram, S., (1997). Combustion synthesis. Current Opinion in Solid State and Materials Science, Vol. 2 (2), pp. 158-165.
- Patil, K., Aruna, S. y Mimani, T., (2002). Combustion synthesis: an update. Current Opinion in Solid State and Materials Science, Vol. 6 (6), pp. 507-512.
- Pérez, M., Lugo, C., Quintero, M., Pérez, P., Villarroel, M., Rodríguez, P., Imbert, F. y Del Castillo, H., (2015). Síntesis de óxidos mixtos tipo perovskitas de $La_xSr_{1-x}Ni_yAl_{1-y}O_3$ preparados vía combustión en solución (SCS). Revista Ciencia e Ingeniería, Vol. 36 (2), pp. 93-104.
- Rahdar, A., Aliahmad M., Azizi Y., (2015). NiO Nanoparticles: Synthesis and Characterization, Journal of Nanostructures, JNS, Vol. 5, 145-151.
- Radev, L., Pavlova, L., Samuneva, B., Kashchieva, E., Mihailova, I., Zaharescu, M., Malic, B., Predoana, L., (2008). Sol-gel synthesis and structure of La_2O_3 - CoO - SiO_2 powders, Processing and Application of Ceramics, Vol. 2(2), 103-108.
- Ramos, K., Jiménez, Y. y Linares C., (2015). Síntesis y caracterización de óxidos MgAl, MgFe, FeAl y MgFeAl para la degradación de fenol con foto-fenton solar. Revista latinoamericana de Metalurgia y Materiales, Vol. 35 (2), pp. 315-325.
- Rendón, J., Moreno, L. y Valencia, J., (2006). Síntesis y caracterización de perovskitas de $LaCoO_3$ por el método citrato. Revista colombiana de Física, Vol. 38 (2), pp. 906-909.
- Rodríguez-Sulbarán, P. J., Lugo, C. A., Perez, M. A., Gonzalez-Cortes, S. L., D'Angelo, R., Rondon, J., ... & Del Castillo, H. L. (2018). Dry reforming of methane on LaSrNiAl perovskite-type structures synthesized by solution combustion. In *Advanced Solid Catalysts for Renewable Energy Production* (pp. 242-266). IGI Global.
- Savinskaya, O., Nemudry, A. y Lyakhov, N., (2007). Synthesis and properties of $SrFe_{1-x}M_xO_{3-z}$ ($M = Mo, W$) perovskites. Inorganic Materials, Vol. 43 (12), pp. 1350-1360.
- Siddique, F., Gonzalez-Cortes, S., Mirzaei, A., Xiao, T., Rafiq, M. A., & Zhang, X. (2022). Solution combustion synthesis: the relevant metrics for producing advanced and nanostructured photocatalysts. Nanoscale, Vol. 14 (33), 11806-11868.
- Sierra, G., Gallego, J., Batiot-Dupeyrat, C., Barrault, J. y Mondragón, F., (2009). Influence of Pr and Ce in dry methane reforming catalysts produced from $La_{1-x}A_xNiO_{3-\delta}$ ($A = Pr, Ce$). *Applied Catalysis A: General*, Vol. 369, (1-2), pp. 97-103.
- Silva, B., Kulesza, J., De Araújo, D. y Kienneman, A., (2015). Nickel-based Catalyst Precursor Prepared Via Microwave-induced Combustion Method: Thermodynamics of Synthesis and Performance in Dry Reforming of CH_4 . *Materials Research*, Vol. 18 (4), pp. 732-739.
- Sithole, M., Omondi, B., & Ndungu, P., (2017). Synthesis and characterization of $Ce_{0.6}Sr_{0.4}Fe_{0.8}Co_{0.2}O_{3-\delta}$ perovskite material: Potential cathode material for low temperature SOFCs. *Journal of Rare Earths*, Vol. 35 (4), 389-397.
- Song, S., Sheptyakov, D., Korsunsky, A., Duong, H. y Lu L., (2016). High Li ion conductivity in a garnet-type solid electrolyte via unusual site occupation of the doping Ca ions. *Materials and Design*, Vol. 93, pp. 232-237.
- Specchia, S., Ciera, A. y Saracco, G., (2004). In situ combustion synthesis of perovskite catalysts for efficient and clean methane premixed metal burners. *Chemical Engineering Science*, Vol. 59 (22-23), pp. 5091-5098.
- Sultana, S., Mohammad, R., Khan, Z., Umar, K., Ahmed, A., & Shahadat, M., (2015). SnO_2 -SrO based nanocomposites and their photocatalytic activity for the treatment of organic pollutants. *Journal of Molecular Structure*, Vol. 1098, 393-399.
- Takeda Y., Kanno R., Sakano M., Yamamoto O., Takano M., Bando Y., Akinaga H., Takita K., Goodenough J.B., (1990). Crystal chemistry and physical properties of $La_{2-x}Sr_xNiO_4$ ($0 \leq x \leq 1.6$), *Materials Research Bulletin*, Vol. 25(3), pp. 293-306.
- Varma, A., Mukasyan, A., Deshpande, K., Pranda, P. y Erii, P., (2003). Combustion Synthesis of Nanoscale Oxide Powders: Mechanism, Characterization and Properties. *Materials Research Society Symposium Proceeding*, Vol. 800, pp. 113-125.
- Villaquirán, C., Medina, C., & Tirado, L., (2015). Effect of cobalt-incorporation on the proper-ties of $Sr_xBa_{1-x}Nb_2O_6$ system. *Ingeniería y Desarrollo*, Vol. 33 (2), 281-300.
- Wade L., (2004). Química Orgánica (quinta edición). Madrid-España: Pearson Educación S.A., 500, 505, 1207.

- Wang, K., Zhong, P. y Zhu, J., (2009). Preparation of Highly Active and Stable Perovskite-like Catalyst by Combustion Method: Effect of Complex. *Catalysis Letters*, Vol. 131, pp. 672-675.
- Zhao, Y., Hong, L., Hong, J. y Zhu, J., (2004). Synthesis of lead sulfide nanocrystals via microwave and sonochemical methods. *Materials Chemistry and Physics*, Vol. 87 (1), pp. 149-153.

Rondón Contreras, Jairo: Doctor in Applied Chemistry, mention Materials Study, 2015, University of the Andes; Professor in the Biomedical & Chemical Engineering Departments at the Polytechnic University of Puerto Rico, San Juan, PR-USA. Email: jrondon@pupr.edu

DOI <https://orcid.org/0000-0002-9738-966X>

Recibido: 16 de julio de 2024

Aceptado: 08 de octubre de 2024

Lugo González, Claudio Antonio: Doctor in Applied Chemistry, mention Materials Studies, 2017, University of the Andes; Professor in the Chemistry Department (Kinetics and Catalysis Laboratory) at the Faculty of Sciences, ULA. Merida, Venezuela.

DOI <https://orcid.org/0000-0001-8003-0354>

Torres Ibarra Rubén Darío: Bachelor's Degree in Chemistry, 2023, Chemistry Department (Kinetics and Catalysis Laboratory) at the Faculty of Sciences, University of the Andes, Mérida, Venezuela. Email: rubendti.16@gmail.com

DOI <https://orcid.org/0009-0000-3600-8571>

Guerrero Rojas, Maryuri: Bachelor's Degree in Chemistry, 2023, Chemistry Department (Kinetics and Catalysis Laboratory) at the Faculty of Sciences, University of the Andes, Mérida, Venezuela. Email: mar94688@gmail.com

DOI <https://orcid.org/0009-0000-8230-7038>

Fereira Chacón, Carla Yanosky: Bachelor's Degree in Chemistry, 2023, Chemistry Department (Kinetics and Catalysis Laboratory) at the Faculty of Sciences, University of the Andes, Mérida, Venezuela. Email: carlayanosky@gmail.com

DOI <https://orcid.org/0009-0004-2961-7802>

Petit Chacón, Eliel José: Bachelor's Degree in Chemistry, 2023, Chemistry Department (Kinetics and Catalysis Laboratory) at the Faculty of Sciences, University of the Andes, Mérida, Venezuela. Email: elielpetit4@gmail.com

DOI <https://orcid.org/0009-0004-3623-2732>

Pérez Dávila, Patricia: Doctor in Drug Chemistry, 2017, Scientific Research Institute, Faculty of Pharmacy and Bioanalysis, University of the Andes; Professor of the Polymer Laboratory in the Faculty of Sciences, ULA. Mérida, Venezuela. Email: perezdpatricia@gmail.com

DOI <https://orcid.org/0000-0003-0591-2351>